The Design of Planar Circulators for Wide-Band Operation

TANROKU MIYOSHI, MEMBER, IEEE, AND SHINICHI MIYAUCHI

Abstract—**The stripline circulator used in microwave integrated circuits (MIC) is considered one of ferrite planar circuits (two-dimensional circuits). We investigated the optimum shape of a planar circulator for wide-band operation, perceiving the wider freedom of the planar structure in circuit design. The wide-band planar circulator, designed using the powerful contour-integral method is triangular shaped with slightly concave sides. The 20-dB isolation fractional bandwidth of the designed circulator is about 52 percent.**

I. Introduction

THE STRIPLINE circulator used in microwave integrated circuits (MIC) is considered to be one of ferrite planar circuits (two-dimensional circuits). We investigated the optimum shape of a planar circulator for wide-band operation, perceiving the wider freedom of the planar structure in circuit design. So far, the octave bandwidth design of a disk-shaped stripline circulator without external tuning elements was presented by Wu and Rosenbaum in 1974 [1] whose analysis was based upon Bosma's Green function method [2]. Although their work made an epoch in the design of a wide-band stripline circulator, there are two problems to be re-examined. First, in their analysis the impedance matrix of the circulator was approximately defined (after Bosma) by using the average voltage and current on each port even for a large junction coupling angle. Second, the possibility of the octave bandwidth operation was predicted but the precise limit of the 20-dB isolation fractional bandwidth of the disk-shaped circulator was not shown clearly. Although Ayter and Ayasli [3] further examined Wu and Rosenbaum's design, only the design curves giving the frequency dependence of the circulation equation was shown. Therefore, we will first discuss the upper limit of the 20-dB isolation fractional bandwidth of the disk-shaped circulator. Next, to find the best shape of a planar circulator for wide-band operation, triangular circulators with various curved sides will be discussed. In our analysis based upon the contour integral method [4], the fields on the ports will be expanded in terms of the stripline modes. Further, to give clearer understandings of the wide-band circulator, such characteristics as the eigenadmittances and the circulator equivalent admittance [5] are also presented.

Manuscript received April 16, 1979; revised October 15, 1979.

The authors are with the Department of Electronic Engineering, Kobe University, Rokko, Nada, Kobe 657 Japan.

II. Numerical Analysis of a Planar Circulator

A triplate planar circulator consists of a rotationally symmetrical thin center conductor sandwiched by two ferrite substrates with magnetic field perpendicular to the ground conductors as shown in Fig. 1. There are three uniform striplines connected to the ferrite planar circuit. All of them are sandwiched by the isotropic dielectric material. The remainder of the periphery is assumed to be open circuited. The xy coordinates and z axis, respectively, are set parallel and perpendicular to the conductors.

When the spacing is much smaller than the wavelength, only the field components E_z, H_x, and H_y with no variation along the z axis are considered. It is deduced directly from Maxwell's equation that the following equation governs the electromagnetic fields in the ferrite planar circuit:

$$(\nabla_T^2 + k^2)V = 0 \tag{1}$$

where

∇_T^2 $= \partial^2/\partial x^2 + \partial^2/\partial y^2$
k $= (\omega/c)(\epsilon_f \mu_{\text{eff}})^{1/2}$
ω angular frequency
ϵ_f relative dielectric constant of ferrite
μ_{eff} $= (\mu^2 - \kappa^2)/\mu =$ *effective permeability of the ferrite*
μ, κ diagonal and off-diagonal coefficients of permeability tensor for magnetization in the z direction.

At a coupling port, the following boundary condition given by the differential equation must apply:

$$j\frac{\kappa}{\mu}\frac{\partial V}{\partial t} + \frac{\partial V}{\partial n} = -j\omega\mu_{\text{eff}} d_f i_n \tag{2}$$

where i_n is the surface current density normal to the periphery and ∂n and ∂t, respectively, are the derivative normal to the periphery and the tangential derivative around the periphery.

Almost at the periphery where the coupling ports are absent, the current flow normal to the periphery is assumed to be zero, i.e., $i_n = 0$.

For a numerical calculation based upon a contour-integral method [4], we divide the periphery into $N = 3m + 3n$ incremental sections and set N sampling points defined at the center of each section as shown in Fig. 2. Here the periphery on each port is also divided into m

0018-9480/80/0300-0210$00.75 ©1980 IEEE

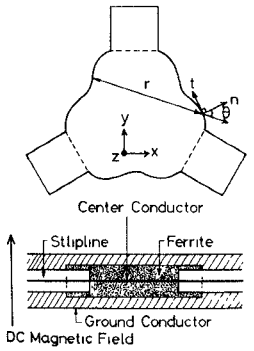

Fig. 1. Triplate planar circulator.

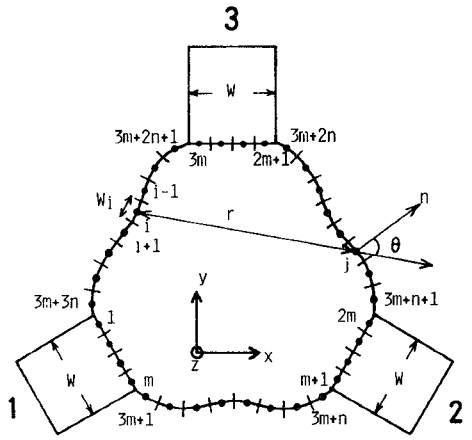

Fig. 2. Center conductor of a planar circulator and symbols used in the numerical calculation.

sections to take the voltage distribution into consideration. In numbering the sampling points, the points on the three ports are first numbered counterclockwise as $1\cdots m$, $m+1\cdots 2m$, and $2m+1\cdots 3m$ and the others at the remainder of the periphery are numbered from $3m+1$ to $3m+3n$. When we assume that the magnetic and electric field intensities are uniform across each section, we obtain a $N\times N$ matrix equation in terms of the RF voltage and the current on the periphery:

$$\sum_{j=1}^{N} u_{ij}V_j = \sum_{j=1}^{N} h_{ij}I_j, \qquad i=1,2,\cdots,N \tag{3}$$

where

$$I_j = -2i_n W_j$$

$$u_{ij} = \delta_{ij} - \frac{k}{2j}\int_{W_j}\left(\cos\theta - j\frac{\kappa}{\mu}\sin\theta\right)H_1^{(2)}(kr)\,dt_j$$

$$h_{ij} = \begin{cases} \dfrac{\omega\mu_{\text{eff}}d_f}{4W_j}\displaystyle\int_{W_j} H_0^{(2)}(kr)\,dt_j, & i\neq j \\ \dfrac{\omega\mu_{\text{eff}}d_f}{4}\left\{1-j\dfrac{2}{\pi}\left(\log\dfrac{kW_i}{4}-1+\gamma\right)\right\}, & i=j \end{cases} \tag{4}$$

$\gamma = 0.5772\cdots$: Euler's constant.

In (4), $H_0^{(2)}$ and $H_1^{(2)}$ are the zeroth-order and first-order Hankel functions of the second kind, respectively. The variable r denotes distance between points i and j and θ denotes the angle made by the straight line from point i and j and the normal at point j as shown in Fig. 2. The formulas u_{ij} and h_{ij} in (4) have been derived assuming that the jth section is straight.

Next, to calculate the circuit parameters of the circulator we approximately expand the RF voltage $V(x)$ and the current density $i_n(x)$ on each port in terms of m stripline modes:

$$V(x) = \sum_{L=1}^{m} v_L \cos(L-1)\pi x/W \tag{5}$$

$$-i_n(x) = \frac{1}{2W}\sum_{L=1}^{m} i_L \cos(L-1)\pi x/W \tag{6}$$

where x is a running coordinate on the port going from 0 to W. v_L and i_L are the expansion coefficients for the Lth higher order mode. The subscript 1 corresponds to the TEM mode. The relations between the expansion coefficients and the RF voltage V_p and the current $I_p = -2i_n W/m (p=1,\cdots,m)$ defined at the sampling points on the port are given by

$$V_i = \sum_{j=1}^{m} A_{ij}v_j \qquad I_i = \sum_{j=1}^{m} A_{ij}i_j/m \tag{7}$$

where

$$A_{ij} = \cos(\pi/2m)(2i-1)(j-1). \tag{8}$$

Since the striplines are assumed to be straight with sufficient length, only the TEM mode can propagate in the uniform stripline and the higher order modes which exist at the port are considered loaded by the reactive characteristic impedance Z_L given by [6]

$$Z_L = -\frac{V_L}{i_L} = jZ_1\left\{\left((L-1)\lambda/2W\sqrt{\epsilon_s}\right)^2 - 1\right\}^{-1/2}$$

$$Z_1 = \frac{60\pi d_s}{W\sqrt{\epsilon_s}} \tag{9}$$

where ϵ_s, d_s, and W are the relative dielectric constant, the thickness, and the width of the stripline, respectively.

From (3), (7), and (9), we can obtain the 3×3 impedance matrix of the circulator, driven by the TEM modes and loaded by the characteristic impedances of the higher order modes.

III. Wide-Band Disk-Shaped Circulator

As mentioned in the Introduction, the upper limit of the 20-dB isolation fractional bandwidth of a disk-shaped circulator is not known clearly. Therefore, we first examined the performance of the circulator[1] using the powerful contour-integral method described so far, and found that the one with a junction coupling angle of about 50° gave the best fractional bandwidth. The computed performance of the circulator is shown in Fig. 3. The 20-dB isolation fractional bandwidth is about 43

[1]Strictly speaking, the contour of a disk-shaped circulator is not a perfect circle but has three straight sections at the ports.

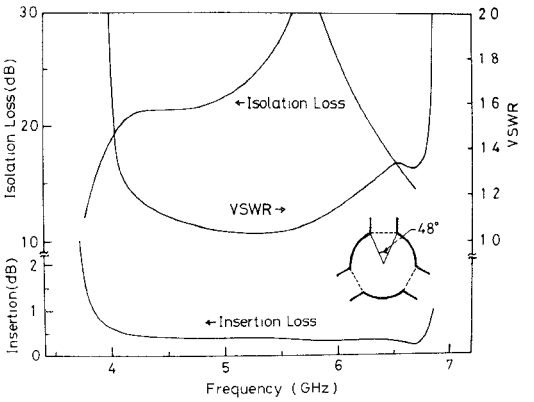

Fig. 3. Computed performance of the best disk-shaped circulator.

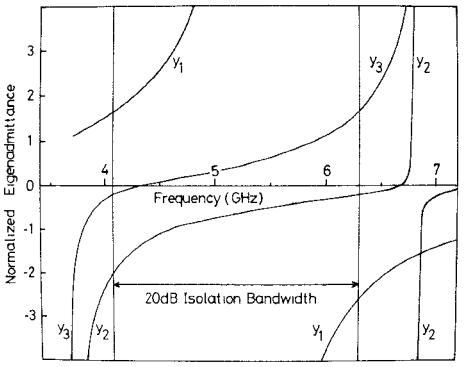

Fig. 4. Normalized eigenadmittances of the disk-shaped circulator shown in Fig. 3. y_1 is for the same phase excitation and y_2 and y_3 correspond to the rotational excitation.

percent, while the VSWR and the insertion loss are less than 1.3 and 0.6 dB, respectively, over the frequency range. The operation ranges are $0.58<|\kappa/\mu|<0.89$ and $2.09>kR>0.76$, where R is the radius of the disk.

To give a clearer understanding of this wide-band circulator, other properties of it will be explained. Fig. 4 shows the eigenadmittances normalized by the characteristic admittance Y_1 of the stripline. They are obtained from the computed elements of the admittance matrix as follows:

$$y_1=(Y_{11}+Y_{12}+Y_{13})/Y_1$$
$$y_2=(Y_{11}+Y_{12}\exp(-j\alpha)+Y_{13}\exp(-2j\alpha))/Y_1$$
$$y_3=(Y_{11}+Y_{12}\exp(j\alpha)+Y_{13}\exp(2j\alpha))/Y_1 \qquad (10)$$

where $\alpha=2\pi/3$, y_1 is the normalized eigenadmittance of the same phase excitation, and y_2 and y_3 are those of the rotational excitation. It is found that over the frequency range having the isolation loss better than 20 dB, the perfect circulation condition is almost satisfied.

Fig. 5 shows the equivalent admittance [5] of the circulator obtained from the eigenadmittances. The equivalent admittance is an essential quantity to describe a circulator when it is supposed to be matched by connecting the two-port external matching network in each circulator arm. From Fig. 5, the normalized equivalent admittance $g+jb$ is found to be about $1+j0$ over the frequency range.

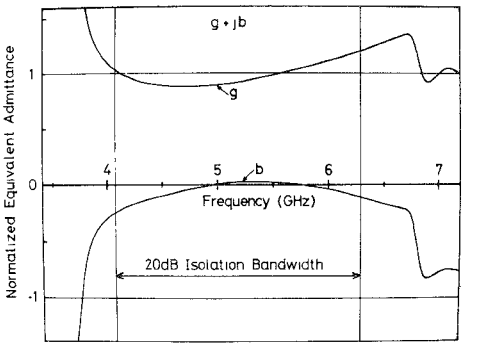

Fig. 5. Normalized equivalent admittance $g+jb$ of the disk-shaped circulator shown in Fig. 3.

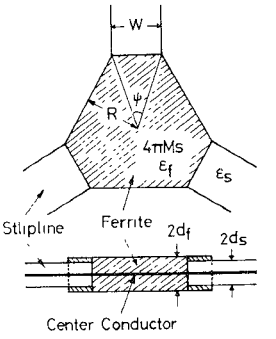

Fig. 6. Structure of a triangular circulator to be optimized.

IV. Wide-Band Planar Circulator

Next, we try to search the best shape of a planar circulator for wide-band operation. To this end, first the optimum parameters of a triangular circulator shown in Fig. 6 will be determined. Thereafter, we will find the best shape by changing the straight sides of the triangle to various curved ones.

A. Determination of Optimum Parameters of a Triangular Circulator

In the numerical optimization of the triangular circulator, the four parameters such as ϵ_s, d_s, R, and ψ are optimized for a specific ferrite material with $4\pi Ms=1300$ G, $\epsilon_f=15.6$, and $d_f=2.0$ mm, that is, just saturated by the dc magnetic field. Fig. 7 shows the computed circulator performance optimized in terms of ϵ_s and d_s for various coupling angles, where R is set equal to 4.6 mm. The best 20-dB isolation fractional bandwidth is found to be about 50 percent for the coupling angle between 35° and 45°. It is worth noting that this value of fractional bandwidth is better than that of the disk-shaped circulator. Helszajn *et al.* also presented the same conclusion as shown here after discussing the loaded Q factors for circulators using disk and triangular planar resonators in [7]. In the numerical calculation, we use 39 sampling points in total along the periphery and set 5 sampling points on each port. In the case of $\psi=36°$, the optimum characteristic impedance of the stripline for the TEM mode is 11.0 Ω, but ϵ_s less than 35 should be adopted to avoid the propagation of the first higher order mode in the stripline. Then the operation

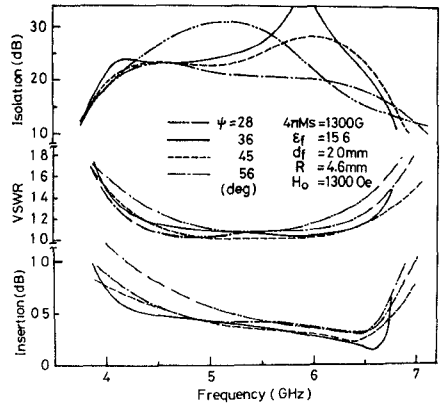

Fig. 7. Computed performances of the triangular circulators optimized in terms of ϵ_s and d_s for various coupling angles.

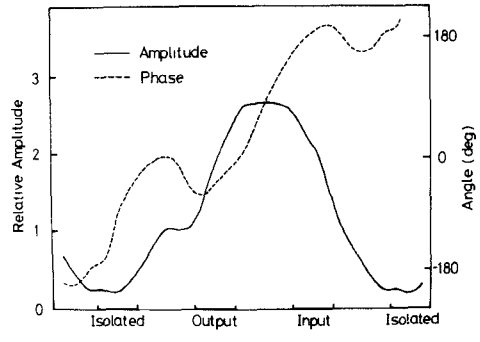

Fig. 8. Computed RF voltage distribution, relative amplitude (solid curve) and phase (broken curve), along the periphery of the triangular circulator with $\psi=36°$ at the center frequency.

ranges are $0.56<|\kappa/\mu|<0.92$, $2.06>kR>0.59$ and the 20-dB isolation fractional bandwidth 49.5 percent. Fig. 8 shows the RF voltage distribution along the periphery of the circulator with $\psi=36°$ at the center frequency. The solid and broken curves show the relative amplitude and the phase of the RF voltage, respectively. It is noticeable that the distribution exhibits no minimum between the input and output ports.

B. Optimum Shape of a Planar Circulator for Wide-Band Operation

Next, we change the straight sides of the optimum triangular circulator to various curved sides to find the best shape of a planar circulator.

Fig. 9 shows the variation of the isolation loss perfomance of the circulators with various convex sides, where all the parameters except shape are kept the same as those of the triangular circulator with $\psi=36°$. To describe the sides, the segments of circles are used. H denotes the greatest distance of the side shown in Fig. 9. It is found from Fig. 9 that the larger H, the worse the fractional bandwidth.

The isolation loss performance of the concave circulators are shown in Fig. 10. From this figure, a circulator with concave sides is expected to realize better fractional bandwidth, if all the parameters are optimized.

In fact, after searching by the trial and error method, we found that the circulator with slightly concave sides

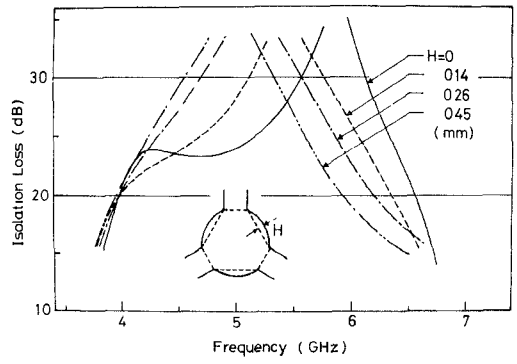

Fig. 9. Variation of the isolation loss performances of circulators with various convex sides. All the parameters except shape are kept the same as those of the triangular circulator with $\psi=36°$. The segments of circles are used to describe the sides.

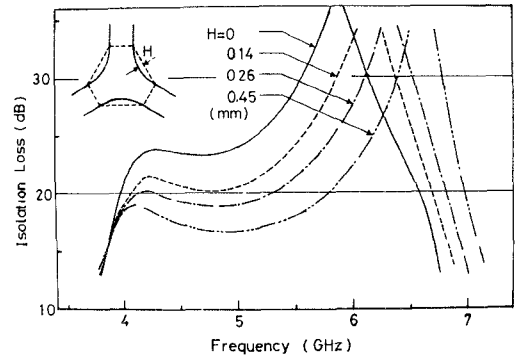

Fig. 10. Computed isolation loss performances of circulators with various cancave sides. The segments of circles are used to describe the sides.

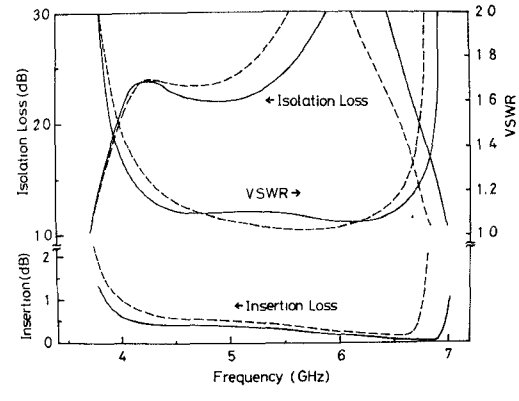

Fig. 11. Computed performance of the best circulator with slightly concave sides, $H/R=0.057$. The broken curves are for the triangular circulator with $\psi=36°$.

gave the best fractional bandwidth. When let R be the radius of the inscribed circle of the original triangle, the ratio of H to R is only 5.7 percent for this circulator. The computed performance of this circulator is shown in solid line curves in Fig. 11 for $Z_1=11.26\ \Omega$. The broken curves are for the triangular circulator. The 20-dB isolation fractional bandwidth is about 52 percent and the operation range is $0.54<|\kappa/\mu|<0.92$. Comparing the two curves, we can see that the perfomance of the concave circulator is improved at higher frequency.

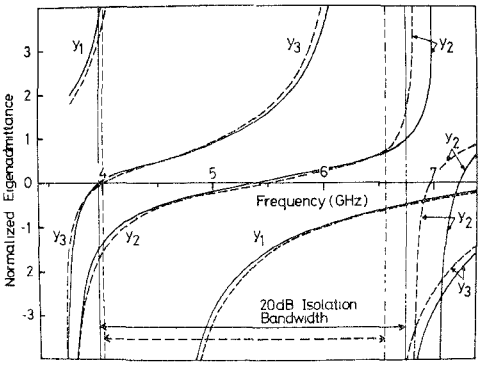

Fig. 12. Normalized eigenadmittances of the designed circulator whose performance is shown in Fig. 11.

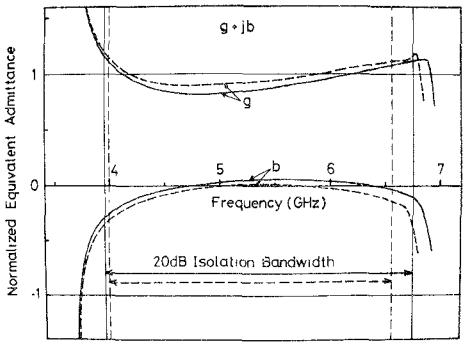

Fig. 13. Normalized equivalent admittance of the designed circulator whose performance is shown in Fig. 11.

The normalized eigenadmittances and the normalized equivalent admittance of this circulator are shown in Fig. 12 and Fig. 13, respectively. The broken curves in the figures are for the triangular circulator with $\psi = 36°$. It is found from Fig. 12 that the improvement of the performance around higher frequency is due to the movement of the second zero point of y_2 to higher frequency.

V. Scaling of Circulator Performance

So far, the optimum parameters have been determined for a specific ferrite material. To design a wide-band circulator at an arbitrary frequency with the same fractional bandwidth as the circulator determined in the previous chapter, it is convenient to use the following scaling rules. They are useful only when the ferrite is just saturated. The scaling rules are the following.

1). As far as the thickness is concerned, the circulator performance depends only upon the ratio d_s/d_f.

2). When R increases m times assuming ϵ_s, ϵ_f, and d_s/d_f are constant, the 20-dB isolation fractional bandwidth does not change only if $f_0 \to f_0/m$ and $4\pi Ms \to 4\pi Ms/\mathrm{m}$.

3). When R increases m times assuming $4\pi Ms$, f_0, and d_s/d_f are constant, the performance does not change only if $\epsilon_s \to \epsilon_s/\mathrm{m}^2$ and $\epsilon_f \to \epsilon_f/\mathrm{m}^2$. Here note that the center frequency f_0 is related to $4\pi Ms$ and R for the designed concave circulator as follows.

$$|\kappa/\mu| = \gamma 4\pi Ms/f_0 = 0.68 \qquad \gamma = 2.8\,\mathrm{MHz/Oe}$$
$$kR = (2\pi f_0/c)\sqrt{\epsilon_f \mu_{\mathrm{eff}}}\; R = 1.50. \tag{11}$$

VI. Conclusion

We have presented the design of a planar circulator for wide-band operation based upon a contour-integral analysis. In conclusion, we think at present that the triangular circulator with the slightly concave sides can realize the best performance for wide-band operation if designed properly.

Acknowledgment

The authors wish to thank Drs. T. Okoshi of University of Tokyo and P. Silvester of McGill University for their encouragement.

References

[1] Y. S. Wu and F. J. Rosenbaum, "Wideband operation of microstrip circulators," *IEEE Trans. Microwave Theory Tech.*, vol. MTT-22, pp. 849–856, Oct. 1974.

[2] H. Bosma, "On stripline Y-circulation at UHF," *IEEE Trans. Microwave Theory Tech.*, vol. MTT-12, pp. 61–72, Jan. 1964.

[3] S. Ayter and Y. Ayasli, "The frequency behavior of stripline circulator junctions," *IEEE Trans. Microwave Theory Tech.*, vol. MTT-26, pp. 197–202, Mar. 1978.

[4] T. Miyoshi, S. Yamaguchi, and S. Goto, "Ferrite planar circuits in microwave integrated circuits," *IEEE Trans. Microwave Theory Tech.*, vol. MTT-25, pp. 593–600, July 1977.

[5] G. P. Riblet, "The measurement of the equivalent admittance of 3-port circulators via an automated measurement system," *IEEE Trans. Microwave Theory Tech.*, vol. MTT-25, pp. 401–405, May 1977.

[6] B. Bianco and S. Ridella, "Nonconventional transmission zeros in distributed rectangular structures," *IEEE Trans. Microwave Theory Tech.*, vol. MTT-20, pp. 297–303, May 1972.

[7] J. Helszajn, D. S. James, and W. T. Nisbet, "Circulators using planar triangular resonators," *IEEE Trans. Microwave Theory Tech.*, vol. MTT-27, pp. 188–193, Feb. 1979.